

Characterization of a Lithium-Ion Solid Dispersion Flow Battery

A Thesis

Presented to
the faculty of the School of Engineering and Applied Science
University of Virginia

in partial fulfillment
of the requirements for the degree

Master of Science

by

Zhaoxiang Qi

December

2015

APPROVAL SHEET

The thesis

is submitted in partial fulfillment of the requirements

for the degree of

Master of Science

AUTHOR

The thesis has been read and approved by the examining committee:

Gary Koenig

Advisor

Geoffrey Geise

Robert Kelly

Accepted for the School of Engineering and Applied Science:

Craig H. Benson, Dean, School of Engineering and Applied Science

December

2015

Print Form

Abstract

A new type of non-aqueous flow battery without carbon additives is proposed and the anolyte chemistry is demonstrated. The so-called “Solid Dispersion Flow Battery” incorporates only solid electroactive materials dispersed in organic lithium-ion battery electrolyte as its flowing suspension. In this work, a unique and systematic characterization approach has been used to study the flow battery electrolyte. An electrolyte laden with $\text{Li}_4\text{Ti}_5\text{O}_{12}$ (LTO) has been characterized in multiple specially designed lithium half cell configurations. The flow battery described in this report has relatively low viscosity for the potential energy density. The lack of carbon additive allows characterization of the electrochemical properties of the electroactive material in flow without the complication of conductive additives and unambiguous observation of the electrorheological coupling in these dispersed particle systems.

List of Figures

Figure 1. Illustration of the mechanism of a lithium ion battery with layer structures of both electrodes.....	2
Figure 2. A schematic of a vanadium redox flow battery.....	5
Figure 3. Schematic illustration of semi-solid flow cell system.....	7
Figure 4. Schematic illustration of solid intercalation particle flow cell system.....	9
Figure 5. Cartoon schematic of cell configurations: (a) a vial cell with the aluminum wire in the LTO suspension as the cathode current collector and the lithium foil in the glass tube as the anode; (b) a flow cell with an aluminum wire current collector in the channel containing the LTO suspension and lithium foil attached on the stainless steel foil as the anode.....	13
Figure 6. XRD patterns for (a) the LTO powder, as well as reference patterns for (b) spinel-phase LTO material (obtained from PDF 00-049-0207) and (c) rutile TiO ₂ (obtained from PDF 00-001-1292).....	15
Figure 7. Scanning electron microscope (SEM) image of the LTO particles.....	17
Figure 8. First discharge and charge cycle of (a) a conventional Li/LTO half cell and (b) a Li/LTO particle coin cell, both charged/discharged at a rate of ~0.1C..	18
Figure 9. Cycling performance of LTO particle coin cells loaded with (a) 5.35, (b) 8.74, (c) 26.75, and (d) 40.14 mg LTO. Cycling currents relative were the same (adjusted for active material mass) for the different LTO loadings. The charge/discharge rates used were 0.1C (first 2 cycles), 0.2C (cycles 3-6), 0.5C	

(cycles 7-10), 1C (cycles 11-14), 2C (cycles 15-18), and 5C (cycles 19-22), and 0.2C (cycles 23-26). 1C assumed to correspond to 174.55 mA g^{-1} for calculation of C rate..... 21

Figure 10. The viscosity as a function of shear rate for the particle-free electrolyte (1.2 M LiPF_6 in EC/EMC = 3:7 solvents, black squares) and the electrolyte laden with 5 (red circles), 10 (blue triangles), and 20 (purple pentagons) vol% LTO....25

Figure 11. (a) Chronoamperometry (CA) profiles at 1.2 V and (b) cyclic voltammetry (CV) scans at the rate of 5 mV s^{-1} for the particle-free electrolyte and the electrolyte laden with 5 (red), 10 (blue), and 20 (purple) vol% LTO as measured in the vial cell. Inset in (a) is the steady state current as a function of the LTO concentration in the suspension.....30

Figure 12. (a) Chronoamperometry (CA) profiles at 1.2 V with the stirring halted during the test, (b) Chronopotentiometry (CP) profiles with applied discharge currents 0.02, 0.05, 0.10 mA, and (c) discharge and charge curves for the vial cell with an LTO concentration of 10 vol%.....33

Figure 13. (a) Chronoamperometry (CA) profile at 1.2 V, (b) cyclic voltammetry (CV) scan at the rate of 5 mV s^{-1} , and (c) discharge and charge curve for the flow cell with an LTO concentration in the electrolyte of 10 vol%.....40

Acknowledgements

I would like to thank my advisor Gary Koenig for his valuable suggestions and inspirations for me through the project. I really enjoyed discussing with him. I also want to thank the members in Koenig's research group, Ethan Paharik, Pierce Robinson, Charles Michaelis and Spring Dong for their help of both valuable discussion and training me to operate various instruments. I give my thanks to Ricky Buchanan for helping me make different designs of flow cells, which are critical for my research. I also thank Prof. David Green for use of his lab's rheometer.

I want to thank all my families and friends for their continuous support, especially my parents Chunmou Qi and Mei Zhang, my little sister Jinghan Qi, my grand parents Quanrong Zhang, Xinzhen Hu, and my girlfriend Cuiting Yang. I cannot have the work done without their support.

This research was supported by the National Science Foundation through award ECCS-1405134 and by start-up support at the University of Virginia. The LTO powder was provided by the U.S. Department of Energy's (DOE) CAMP (Cell Analysis, Modeling and Prototyping) Facility, Argonne National Laboratory. The CAMP Facility is fully supported by the DOE Vehicle Technologies Program (VTP) within the core funding of the Applied Battery Research (ABR) for Transportation Program.

Table of Contents

Abstract.....	i
List of Figures	ii
Acknowledgements.....	iv
Table of Contents.....	v
1. Introduction	1
1.1. Lithium-Ion Batteries.....	1
1.2. Redox Flow Batteries	4
1.3. Semi-Solid Flow Battery	6
1.4. Research Objectives	8
2. Experimental Methodology	11
2.1. Preparation and Characterization of Materials	11
2.2. Electrochemical Characterization	11
2.3. Vial Cell and Flow Cell Testing	12
3. Results and Discussions	15
3.1. Materials Characterization	15
3.2. Conventional Coin Cell Electrochemical Characterization.....	17
3.3. Particle Coin Cell Electrochemical Characterization	19
3.4. Rheological Characterization	24
3.5. Vial Cell Electrochemical Characterization.....	28
3.6. Flow Cell Electrochemical Characterization	38
4. Conclusions and Recommendations.....	44
5. References	46

1. Introduction

Due to environmental concerns over the use of fossil fuels and their resource constraints, renewable energy sources such as solar and wind have attracted more and more attention [1]. The intermittent nature of these renewable sources, such as day/night cycles and weather variation, however, causes significant challenges for the electric grid operators because other power plants (usually fossil fueled power plants) need to compensate for the dramatic change in power supply [1, 2]. To further reduce the usage of fossil fuels, large scale energy storage technologies are needed to store electrical energy and improve the energy quality from the renewable energies effectively at a low cost [3]. Pumped-hydro energy storage (PHES) and compressed air energy storage (CAES) are the only two large scale technologies commercially available for grid electricity storage, but they are limited by either poor long term efficiency or geographic limitations [4, 5]. Electric Vehicle is another application that requires relatively large-scale electric energy storage devices. In the electric vehicles, durability, and cost are the key limiting factors besides safety [6]. There is the recognition that battery systems can offer a number of high-value opportunities for large scale energy storage [5].

1.1. Lithium-Ion Batteries

Rechargeable batteries are another group of energy storage devices which come in many forms. Commonly used types are lead acid, nickel cadmium, nickel

metal hydride, and lithium ion. Chemical battery systems are constantly being developed, such as sodium sulfur, lithium sulfur, lithium air, and liquid metal [7-10]. The basic way that rechargeable batteries work is to charge the batteries by transferring electrons to the anode to store electrical energy. The battery can be discharged to provide electromotive force (EMF) to utilize the stored electrical energy.

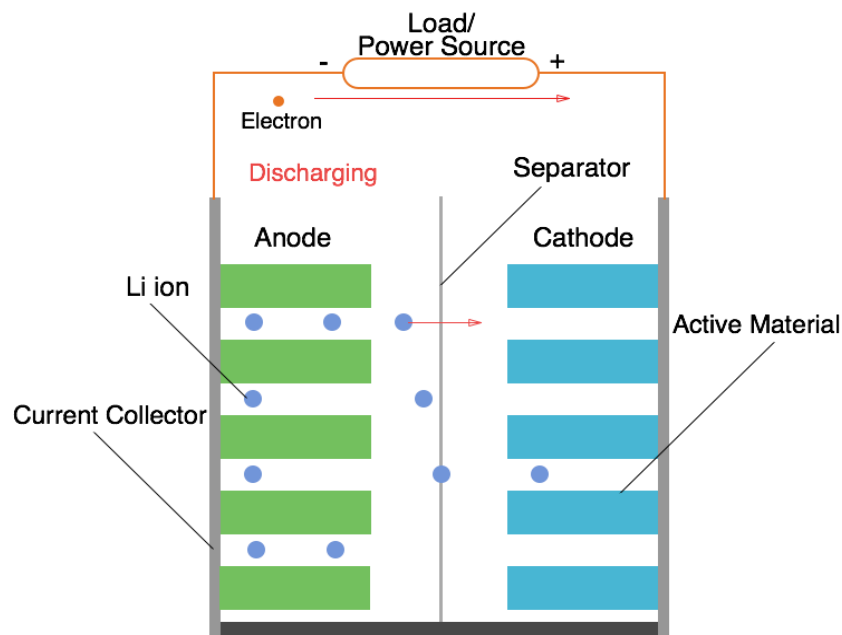
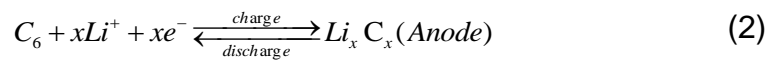
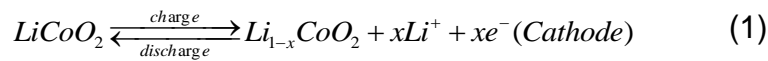


Figure 1. Illustration of the mechanism of a lithium ion battery with layer structures of both electrodes.

Among the known battery chemistries, lithium-ion batteries offer the highest energy density and thus are the major contenders for both stationary and transportation applications [11, 12]. As shown in Figure 1, a typical lithium ion battery consists of current collectors, anode and cathode (negative and positive) active materials, separator, and electrolyte. Current collectors conduct electrons between the battery and the external circuit. Active materials are the component

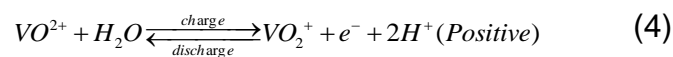
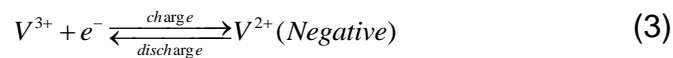
that store the electrical charge, in this case the lithium ions. The separator not only prevents a short circuit, but also provides pathways for lithium ions to transfer between the anode and cathode. The electrolyte consists of solvents with dissolved lithium ions. For a graphite/lithium cobalt oxide battery, the most popular battery used in cell phones and laptops, the anode material is graphite and the cathode material is lithium cobalt oxide (LiCoO₂). As indicated in Equation 1 and Equation 2, lithium ions are pulled out from the cathode and transferred to the anode during the charging process. Lithium ions go the opposite way when being charged. The amount of lithium ions stored and cycled in the system determines the capacity of the battery, typically reported in milliamp-hours (mAh).



To improve the energy density and cycling efficiency of the batteries, different electrode materials and crystal structures have been developed [11, 13-15]. Conventional rechargeable batteries offer a simple and efficient way to store electricity, but development to date has largely focused on smaller systems [3]. The cell performance, such as rate capability and safety, is limited by the mass transport limitations of the ions in the electrolyte [16]. Thus the only way to scale up conventional batteries is to stack many small batteries together, which raises the overall cost due to the need for complicated heat removal system and battery management system [17-20].

1.2. Redox Flow Batteries

A different approach is to decouple the energy storage part and the power output. A representative technology is redox flow battery. Redox flow batteries are typically comprised of active electrochemical cells, pumping system and energy storage tanks with transition metal redox couples dissolved in highly acidic aqueous electrolytes [3, 21]. A schematic of this battery is shown in Figure 2 for the case of a vanadium redox flow battery, which is the most popular and successfully commercialized redox flow battery [22]. Electrolytes with dissolved active molecules are stored in external tanks rather than assembled with the current collectors and the separator. While charging or discharging, the anolytes and catholytes are being pumped through the electrochemical cell and the redox reactions occur simultaneously in both half cells. The reactions are indicated in Equation 3 and 4. Redox flow batteries are ideal for large scale energy storage because of the decoupling of the power and the energy in the system, which provides the flexibility to independently adjust and design the power and energy requirements for an application [23]. The electrochemical energy is stored in electrolyte tanks, which in principle results in total energy only being limited by tank size.



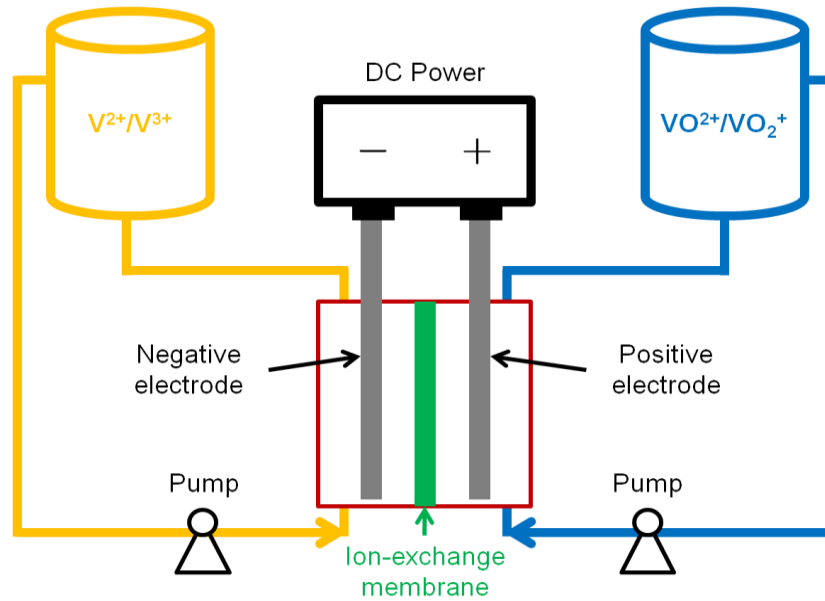


Figure 2. A schematic of a vanadium redox flow battery [22].

The energy density in conventional flow batteries, however, is highly limited by the solubility of the active species, because beyond the solubility limit inactive precipitates form in the electrolyte [3, 21]. Different approaches have been pursued in the literature to improve flow battery performance, including investigating new redox couples [22], designing more efficient current collectors [23-26], incorporating electrolyte additives [27], and modifying the ion-transferring membrane [28]. The long-term performance or cycle life of these systems is also limited by the significant loss of stored energy (i.e., capacity loss) in the electrolytes over time due to transport of the active species across the separator [28], and safety issues are also a concern because sulfuric acid is used as the flowing electrolyte.

1.3. Semi-Solid Flow Battery

Alternative flow battery systems beyond the conventional dissolved transition metal electrolytes have also been reported in the literature such as lead-based flow batteries with soluble lead [29] or polymer suspensions [30]. Another modified flow battery that has been developed is a convection battery with the electroactive materials fixed and electrolyte flowing to improve the mass transport of ionic species in the electrolyte [31, 32]. These reported systems, however, have performance limitations due to maximum practical electrode thicknesses or the inefficient pumping due to high pressure drop. More recently, the possibility of combining lithium-ion battery chemistries with flow batteries has been proposed due to the high energy density and high operating voltages of the active electrode materials [5]. While energy density is not necessarily a major concern for some stationary applications, higher energy density flow battery chemistries will be needed for flow batteries to be implemented in electric vehicles or stationary applications in urban areas where space is limited and energy demand is high. Thus, lithium-ion chemistries have started to be explored for flow battery applications. In some cases the active electrolyte materials are still soluble compounds, for example in the report of a membrane-free semiliquid flow battery composed of a ferrocene-based catholyte and a passivated metallic Li anode [33].

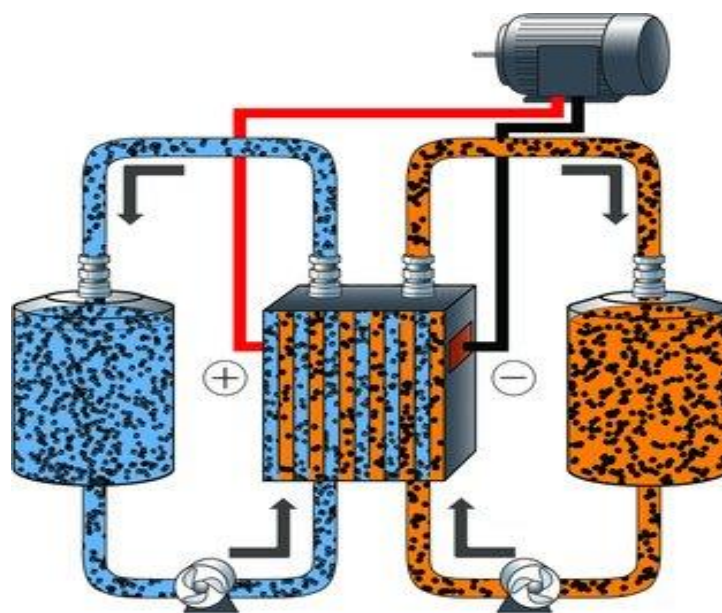


Figure 3. Schematic illustration of semi-solid flow cell system [34].

Other groups have moved to solid electroactive material flow battery designs, and recently the concept of semi-solid flow cells (SSFC) was demonstrated by Chiang's group for both organic and inorganic systems [34, 35]. As shown in Figure 3, electrochemically active particles are suspended in the electrolytes together with conductive carbon, which forms an interconnected network structure with relatively high conductivity. Other research groups have expanded on this concept and incorporated different chemistries into SSFC-type systems, including even highly nonconductive LiFePO_4 [36]. These SSFC-type systems have also explored improvements to the system by incorporation of surfactants within the electrolyte and in developing models of the electrochemical attributes of these flow battery concepts [37, 38]. Compared with the other redox flow battery designs, a high energy storage density ($> 130 \text{ Wh kg}^{-1}$) could potentially be achieved in these SSFC-type systems as a result of the high energy density

solid electroactive materials [34]. However, the operating cost of these SSFC-type systems will likely be extremely high due to the high viscosities ($> 1 \text{ Pa}\cdot\text{s}$ at the shear rate of 35 s^{-1}) of the viscous electrolyte suspensions being pumped through the system [34, 39]. The energy density is also reduced by the addition of carbon additive.

1.4. Research Objectives

Herein, we aim to demonstrate a new type of flow battery without carbon additives and hence with a relatively low viscosity and high energy density. The functional design of the system is similar to a redox flow battery or a SSFC, but the flowing suspension was comprised of only electroactive material particles dispersed into an organic lithium-ion battery electrolyte as shown in Figure 4. In contrast to previous SSFC reports, electrochemical charge/discharge of our flow battery does not rely on an interconnected particle network throughout the electrolyte, but instead relies on the collisions of particles directly in contact with the current collector (or particles in contact with the particles in contact with the current collector). For this initial experimental work, we took advantage of a lithium half cell configuration to characterize an electrolyte laden with $\text{Li}_4\text{Ti}_5\text{O}_{12}$ (LTO). LTO was chosen because of its high capacity (theoretically $174.55 \text{ mAh g}^{-1}$) and good electrochemical performance at a variety of charge/discharge rates [40-42]. The flat charge/discharge profile for LTO should be advantageous at providing a consistent voltage during charge/discharge, regardless of the state of lithiation of the active material in contact with the current collector at any given

time. LTO is also a zero-strain lithium insertion material [43, 44], which prevents fractures of the particles and ensures a stable pressure of the suspension and hence is beneficial to the stability of the suspension. In addition, the charge/discharge potential of LTO (~ 1.55 V vs. Li/Li⁺) is within the stability window of the electrolyte, which removes the complication of significant electrolyte decomposition and solid-electrolyte interphase formation which would be required for other anode materials such as graphite before reversible lithium insertion [45].

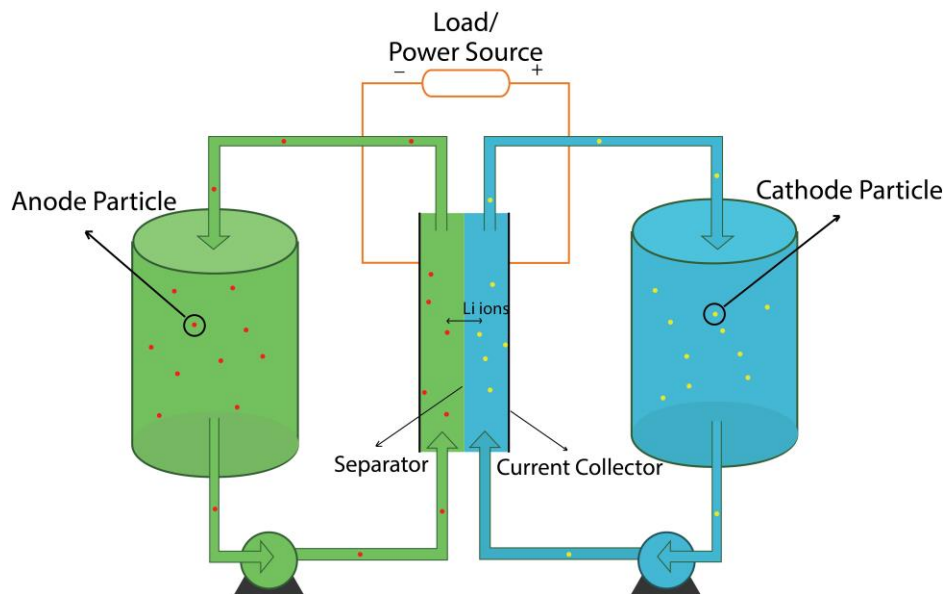


Figure 4. Schematic illustration of solid intercalation particle flow cell system.

Since the system is derived from conventional lithium-ion batteries, we adopted a distinct approach to demonstrate the as-proposed flow battery step-by-step. A conventional lithium-ion battery coin cell was prepared as a benchmark, and then a particle coin cell was constructed free of binders and conductive additives to show that the LTO active material could be successfully charged and discharged

through direct contact with the current collector. After that, a vial cell was prepared to electrochemically characterize the LTO suspension during electrochemical cycling in a turbid flowing environment, and eventually a flow cell was assembled to finally demonstrate the as-proposed flow battery. Rheological tests were also conducted to demonstrate the viscosity of our particle-laden electrolyte as a function of particle loading and relative to other flow battery systems.

2. Experimental Methodology

2.1. Preparation and Characterization of Materials

$\text{Li}_4\text{Ti}_5\text{O}_{12}$ (LTO, NEI Corporation) powders were obtained from the U.S. Department of Energy's (DOE) CAMP (Cell Analysis, Modeling, and Prototyping) Facility, Argonne National Laboratory. The electrolyte (BASF Corporation) was 1.2 M lithium hexafluorophosphate (LiPF_6) in ethylene carbonate (EC) and ethyl methyl carbonate (EMC) with EC/EMC = 3:7 by volume ratio. The LTO suspensions of different loadings (5 vol%, 10 vol%, 20 vol%) were prepared by mixing the LTO powders with electrolyte under stirring overnight, within an argon-filled glove box (with concentrations of $\text{O}_2 < 1$ ppm and $\text{H}_2\text{O} < 1$ ppm) at room temperature.

To characterize the LTO powder morphologies, scanning electron microscope (SEM) images were taken with a Quanta 650 SEM. X-ray diffraction (XRD) patterns were obtained with a Panalytical X'pert diffractometer using Cu K α radiation. Rheology testing of the LTO suspensions was performed with an Anton Paar rheometer (Physica MCR 301, with a 5 cm plate-plate geometry).

2.2. Electrochemical Characterization

A conventional LTO electrode was fabricated from a slurry comprised of 80 wt % LTO powder, 10 wt % carbon black as conductive additive, and 10 wt % polyvinylidene fluoride binder (PVDF) dissolved in N-methylpyrrolidone (NMP, Sigma-Aldrich®). The slurry was agitated in a slurry mixer for 5 minutes and

pasted (with a doctor blade with a gap height of 200 μm) onto aluminum foil. The pasted slurry was dried in an oven at 70 $^{\circ}\text{C}$ overnight and further dried in a vacuum oven at 70 $^{\circ}\text{C}$ for 3 hrs. Electrodes composed of only LTO particles as the electrode material without binders or conductive additives on the aluminum foil were also prepared. LTO particles were suspended in acetone (Fisher Scientific), with a concentration of $\sim 50 \text{ mg mL}^{-1}$, dropped on pre-punched aluminum foil discs (1.6 cm^2), and dried in a vacuum oven at 70 $^{\circ}\text{C}$ for 2 hrs. A coin cell using the as-prepared electrode was referred to as a “particle coin cell”. All coin cells were assembled in the argon-filled glove box. LTO half cells were assembled with the LTO electrode as the cathode and lithium foil as the anode. The electrodes were separated by a polypropylene/polyethylene/polypropylene trilayer membrane. The galvanostatic charge-discharge cycling of coin cells was performed on a Maccor battery cycler.

2.3. Vial Cell and Flow Cell Testing

A customized cell was set up in the glove box as illustrated in Figure 5a, which we refer to as a “vial cell”. An aluminum wire (99.999%, Alfa Aesar) of 1.5 mm in diameter and 20 cm in length was immersed in an LTO suspension of desired particle loading. The lithium foil, which was attached to a copper foil and extended to the external circuit, was immersed into the electrolyte within a glass tube and separated from the LTO suspension by a trilayer membrane separator.

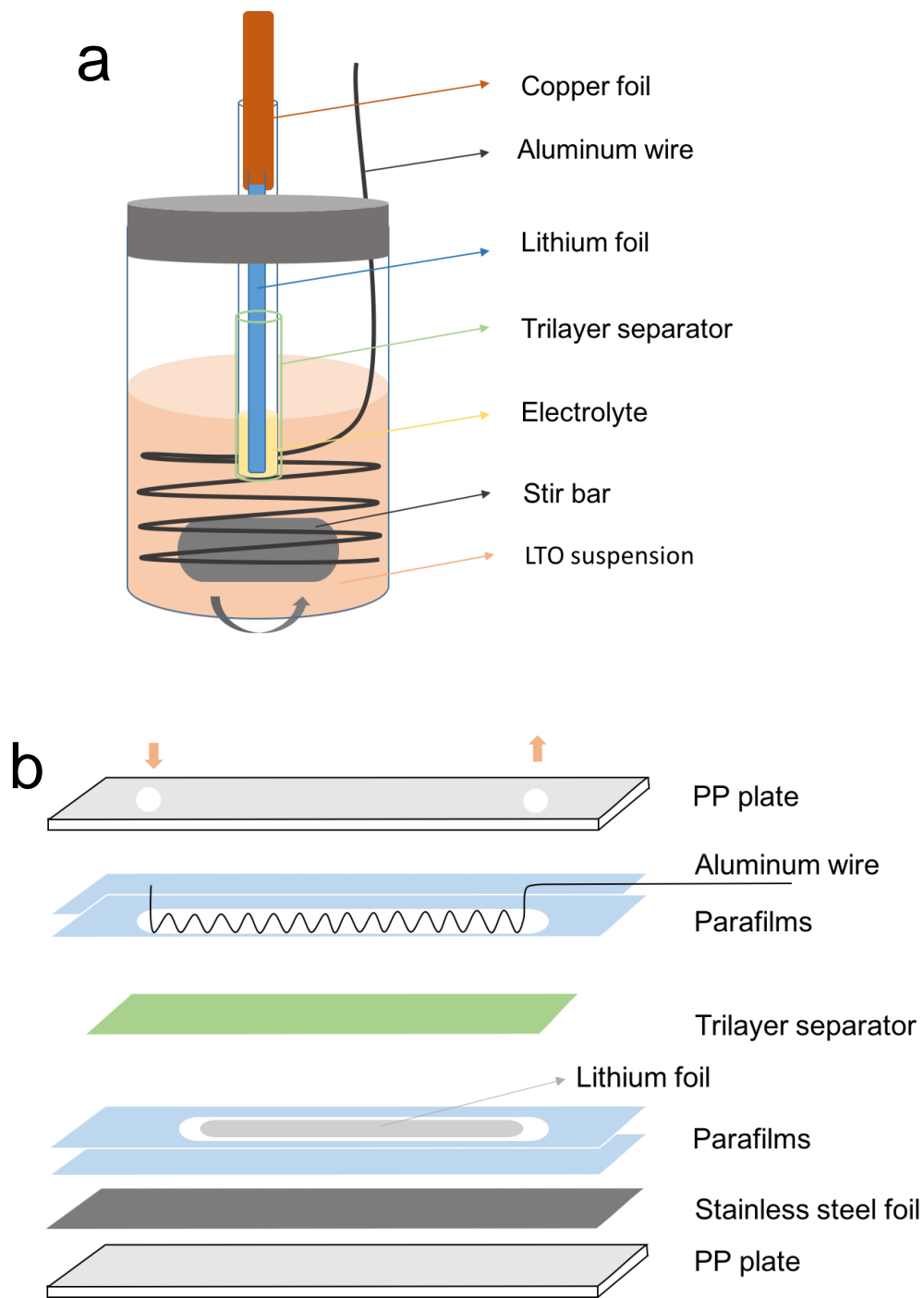


Figure 5. Cartoon schematic of cell configurations: (a) a vial cell with the aluminum wire in the LTO suspension as the cathode current collector and the lithium foil in the glass tube as the anode; (b) a flow cell with an aluminum wire current collector in the channel containing the LTO suspension and lithium foil attached on the stainless steel foil as the anode.

A customized flow cell was set up as illustrated in Figure 5b. The flow channels were formed by cutting compact stacks of laboratory films (Parafilm®) to provide the desired spacing and trilayer membrane separators were used. An aluminum wire (99.999%, Alfa Aesar) of 0.5 mm in diameter and 20 cm in length was assembled in the flow channel as the cathode current collector. A piece of lithium foil was attached on a stainless steel foil (McMaster-Carr) as the anode and connected to a potentiostat (Bio-Logic, SP-150) to perform electrochemical tests. The whole cell was sealed with two polypropylene plates (McMaster-Carr), one on each side. Electrochemical tests for both the vial cell and flow cell were performed within the argon-filled glove box using a Bio-Logic potentiostat (model SP-150).

3. Results and Discussions

3.1. Materials Characterization

As discussed in the Introduction, lithium titanium oxide ($\text{Li}_4\text{Ti}_5\text{O}_{12}$, LTO) was chosen to be evaluated as the electrode material for our system. In practice, we expect this will be used as an anolyte in a full cell with both catholyte and anolyte relying on solid particles for electrochemical energy storage. Before evaluation of LTO in our custom electrochemical cell geometries, we conducted more conventional material and electrochemical characterization on the LTO powder used.

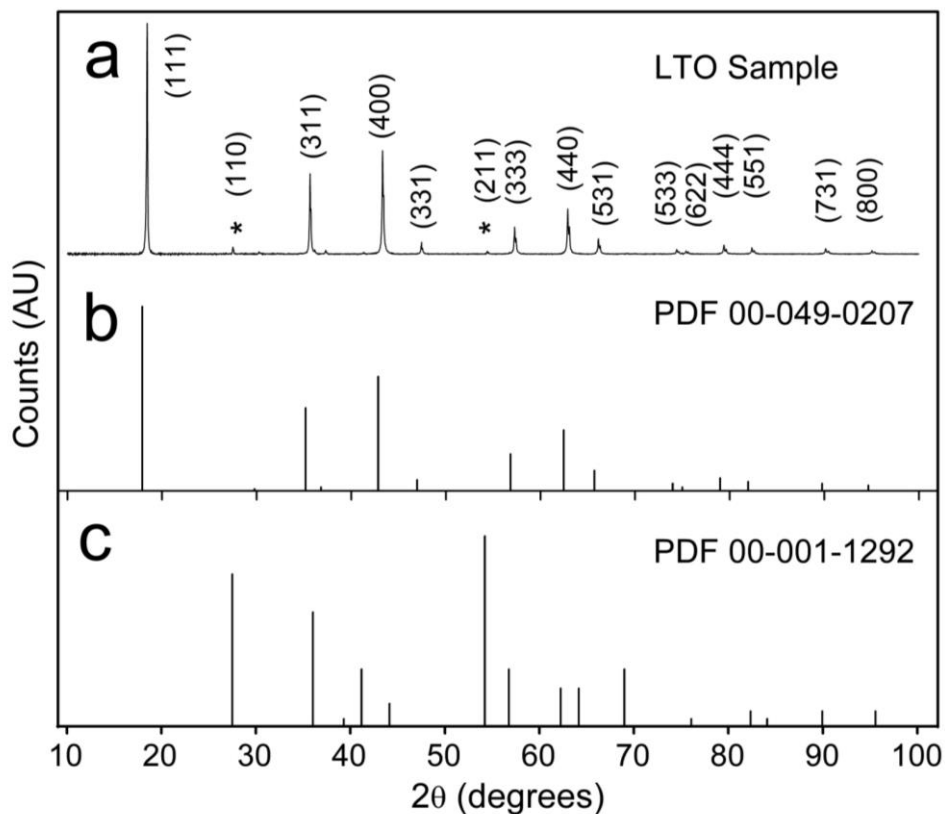


Figure 6. XRD patterns for (a) the LTO powder, as well as reference patterns for (b) spinel-phase LTO material (obtained from PDF 00-049-0207) and (c) rutile TiO₂ (obtained from PDF 00-001-1292).

Figure 6 shows XRD patterns for the LTO powder (Figure 6a), as well as reference patterns for spinel phase LTO material (Figure 6b, obtained from PDF 00-049-0207 [46]) and rutile TiO₂ (Figure 6c, obtained from PDF 00-001-1292 [47]). The peaks for the LTO powder are consistent with the majority of the powder being spinel phase LTO. There are two small but distinguishable peaks in the XRD pattern at 27.49° and 54.36°, which are consistent with an impurity rutile TiO₂ phase also being present in the LTO powder. Rutile TiO₂ impurity is a common impurity observed for LTO materials, and has been reported as an intermediate compound during solid-state synthesis of LTO using anatase TiO₂ and Li₂CO₃ [48, 49]. The morphology of the LTO powder can be seen in the SEM image shown in Figure 7. As can be seen in the image, the LTO powder consisted of irregularly shaped particulates. The average length of the particles, as measured in the SEM image, was 340 ± 200 nm (based on the measured lengths of 35 particles). The XRD and SEM results for the LTO material was consistent with other reports from the literature [50].

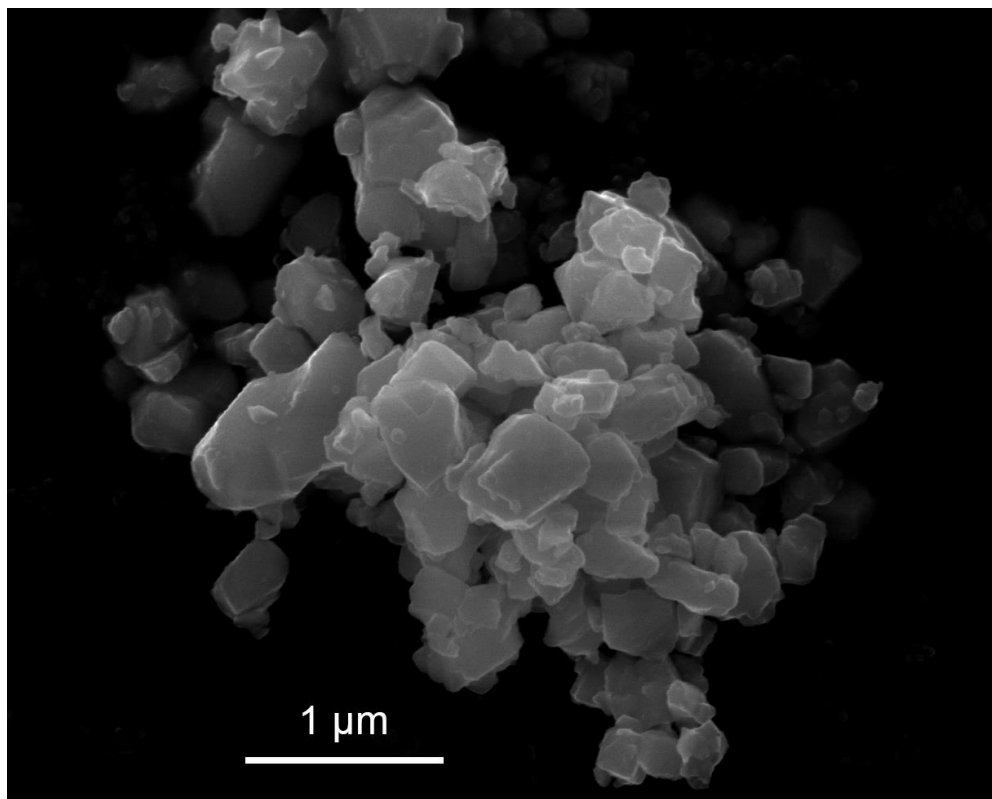
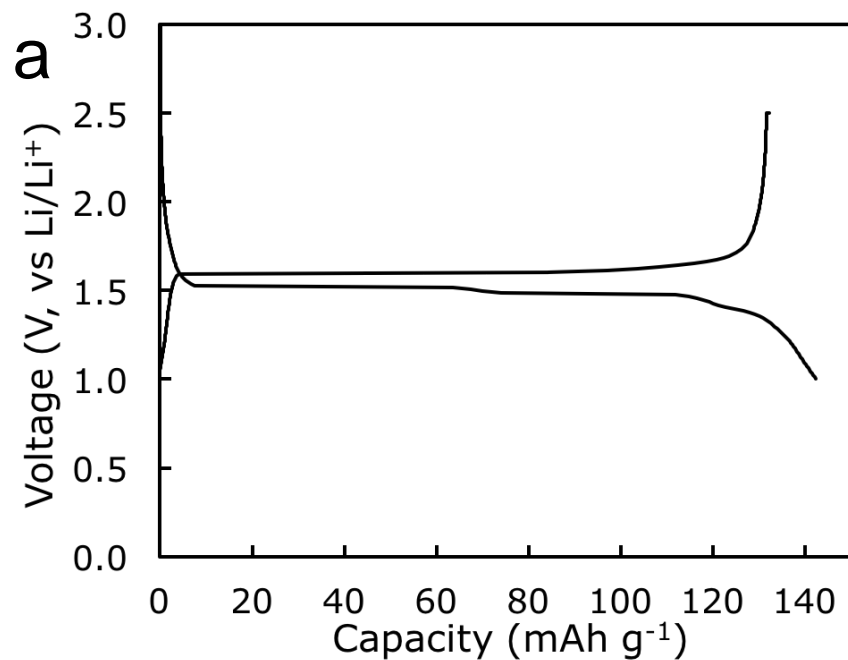


Figure 7. Scanning electron microscope (SEM) image of the LTO particles.

3.2. Conventional Coin Cell Electrochemical Characterization

Before using the LTO powder in our custom electrochemical cell geometries, we evaluated the electrochemical performance of the LTO in conventional composite electrode architectures within coin cells paired with a lithium metal anode. The composite LTO electrodes used in these coin cells were comprised of the LTO powder, conductive carbon additive, and binder as described in the Experimental section. The first discharge and charge cycle of a conventional Li/LTO half cell is shown in Figure 8a. This cell was cycled at a rate of 0.1C (1C assumed to be 174.55 mA g^{-1} based on the theoretical capacity of LTO) and had a first cycle discharge capacity of 142 mAh g^{-1} and charge capacity of 132 mAh g^{-1} . While

the first cycle had 7.12% irreversible capacity loss, the columbic efficiency of subsequent cycles at 0.1C was > 96%. The LTO electrode had a flat charge/discharge plateau at approximately 1.55 V (vs. Li), consistent with other reports in the literature [40, 41, 51-53]. Interestingly, even though the XRD patterns provided evidence of rutile TiO₂ (Figure 6), we did not observe discharge plateaus at 1.4 and 1.1 V which are commonly observed when cycling rutile TiO₂ [54]. This phenomenon was attributed to the small amount of the rutile TiO₂ impurities and the location of rutile TiO₂ phase possibly being segregated within the particle cores, making the rutile phase more difficult for lithium ions to access [49, 55].



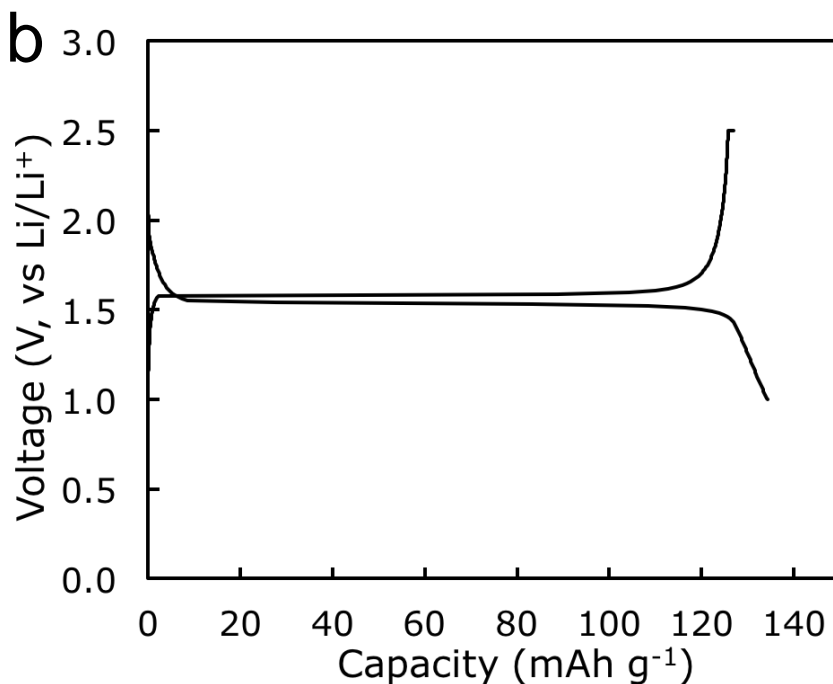


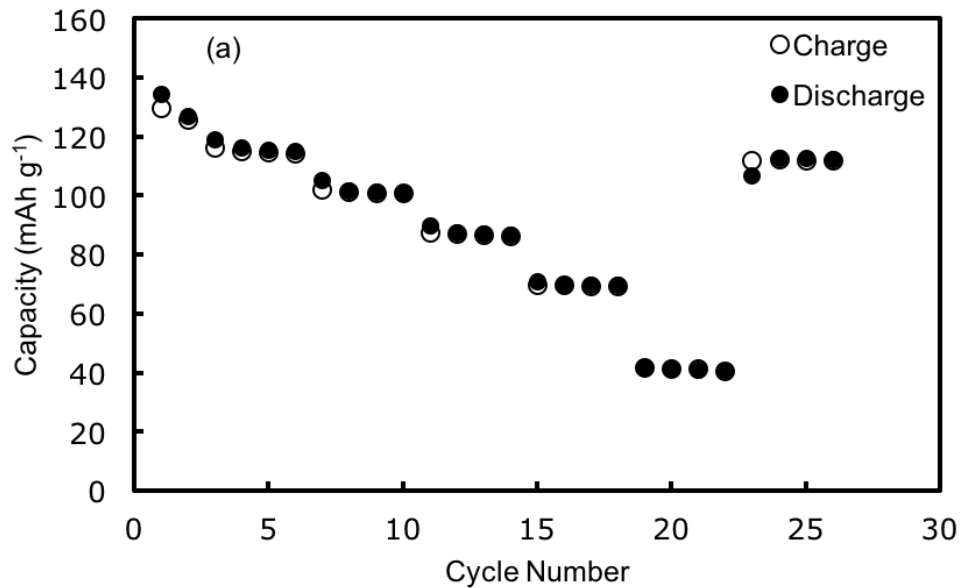
Figure 8. First discharge and charge cycle of (a) a conventional Li/LTO half cell and (b) a Li/LTO particle coin cell, both charged/discharged at a rate of $\sim 0.1C$.

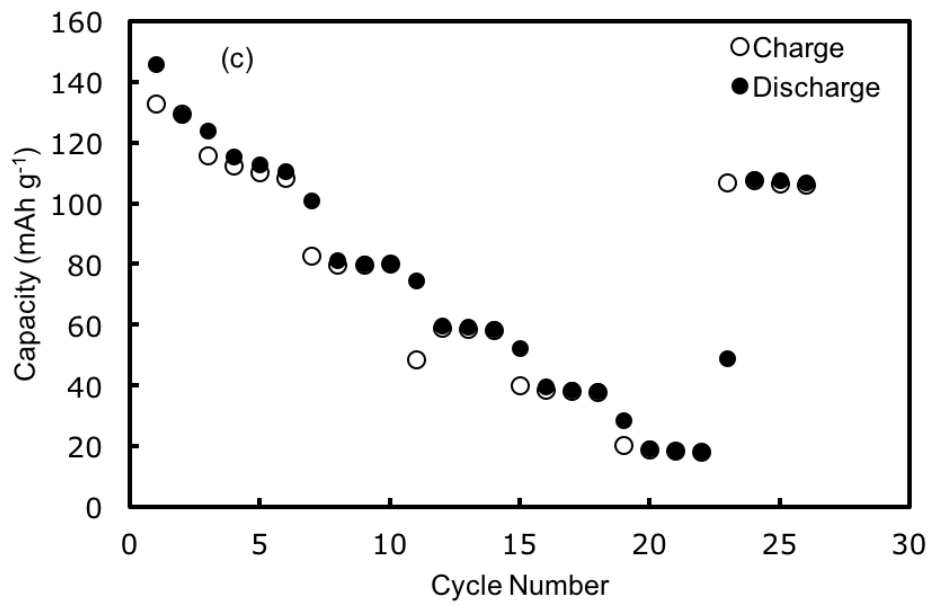
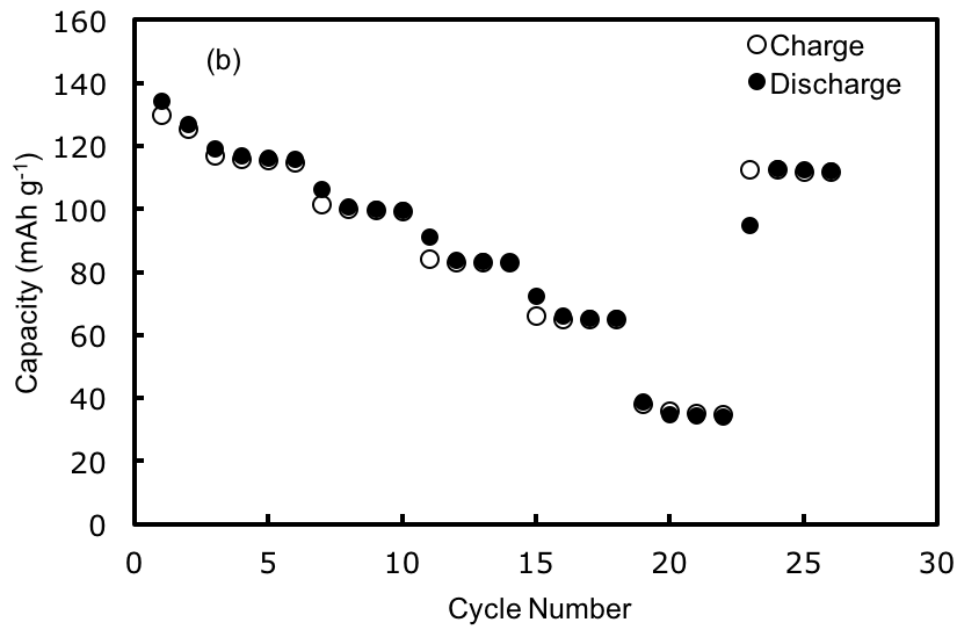
3.3. Particle Coin Cell Electrochemical Characterization

The dispersed particle flow battery that is the focus of this effort relies on active material contact and electrochemical reaction with current collectors in the absence of conductive additives and binders used in fabricating conventional coin cell electrodes. To confirm that our LTO active material could maintain electrochemical activity in the absence of binders and conductive additives, we first fabricated a static battery where the electrode was comprised of only the LTO powder. The method for fabricating what we refer to as “particle coin cells” is described in the Experimental section. The first charge/discharge cycle at a constant charge/discharge rate of $0.1C$ is shown in Figure 8b. This was the same

rate (adjusted for active LTO mass) used for the conventional coin cells described earlier. The initial discharge capacity was 134 mAh g^{-1} , while the charge capacity was 127 mAh g^{-1} . Although the first cycle had 5.50% irreversible capacity loss, the coulombic efficiency of subsequent cycles at 0.1C was ~99%. These results were consistent with other reports from the literature for conventional LTO coin cells [56, 57]. The particle coin cell electrodes prepared for the tests had a thickness of more than $70 \text{ }\mu\text{m}$, which was far greater than the length scale of the particles ($340 \pm 200 \text{ nm}$). The fact that the cell capacity was comparable to the gravimetric value of the conventional coin cell indicated that almost all the LTO in the particle coin cells was participating in electrochemical reactions, including LTO particles that were separated from the current collector by many layers of other LTO particles. Thus, multiple layers of LTO particles on the electrode were electrochemically active rather than just the single layer in direct contact with the current collector. The electrochemical gravimetric capacity of the particle coin cells supports the conclusion that LTO particles are not limited to only participating in electrochemical reactions if they are in direct contact with the current collector. Thus, LTO-to-LTO particle contacts provide sufficient electronic conductivity to allow particles multiple LTO particle distances from the current collector to contribute to battery capacity. Electrodes of different LTO loadings (and hence different thicknesses) were also prepared and tested (Shown in Figure 9). An inverse relationship was observed between particle loading and rate capability of the particle coin cells. Thus, there are limits to the electrochemical capacity that can be extracted from particles far from the current

collector, particularly at higher rates of charge/discharge. This was likely due to the increased resistance experienced by the electrons that had to traverse the extra distance via particle-to-particle LTO contact, as well as the lower lithium-ion accessibility to LTO close to the current collector for the thicker films. These results above, when combined, indicate that the LTO particles should be able to cycle when in contact with the current collector in the flow cell, and that capacity can also be contributed by particles far from the current collector if particle loadings are high enough to allow aggregates of particles that are interconnected to come into contact with the current collector.





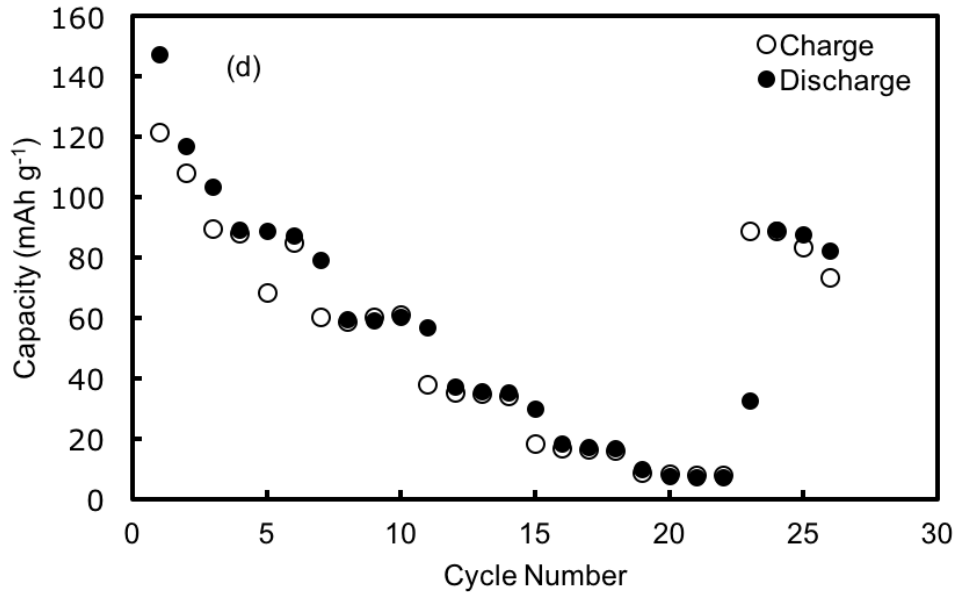


Figure 9. Cycling performance of LTO particle coin cells loaded with (a) 5.35, (b) 8.74, (c) 26.75, and (d) 40.14 mg LTO. Cycling currents relative were the same (adjusted for active material mass) for the different LTO loadings. The charge/discharge rates used were 0.1C (first 2 cycles), 0.2C (cycles 3-6), 0.5C (cycles 7-10), 1C (cycles 11-14), 2C (cycles 15-18), and 5C (cycles 19-22), and 0.2C (cycles 23-26). 1C assumed to correspond to 174.55 mA g⁻¹ for calculation of C rate.

The charge/discharge voltages for the particle coin cells were very flat with plateaus near 1.55 V, indicating minimal electrode polarization. Interestingly, the particle coin cell had an even lower difference between the average charge and discharge potentials, even though the particle cell does not contain conductive additives or binders. We attribute this observation to the excellent electronic and ionic conductivity of LTO material [58]. Although the initial electrical conductivity of LTO has been reported to be $10^{-6} \sim 10^{-13} \text{ S cm}^{-1}$ [59], the conductivity has been demonstrated to rise sharply to 10^0 S cm^{-1} after very low levels of lithiation and can be regarded as a conductor [58]. The electrochemical performance of the

particle coin cells demonstrated that conductive additives were not necessary to effectively charge and discharge the LTO material when in contact with the current collector. These results provided additional motivation that a flow battery of LTO dispersed in electrolyte could be effectively charged and discharged through the contact of LTO particles with the current collector.

3.4. Rheological Characterization

Before evaluating the LTO material in custom flow geometries, we determined the rheological properties of LTO powder dispersed into the electrolyte. The rheological properties of a dispersed flow battery system are important both from an energy efficiency perspective and from a performance perspective. With regards to energy efficiency, the higher the viscosity of the particle-laden suspensions, the greater the energy demands of the pumps to move the particle dispersion through the flow battery system. Assuming the energy to drive the pumps is also provided by the flow battery, this parasitic energy loss will need to be considered in optimization of the overall energy efficiency of the battery [39]. Some slurry flow batteries have extremely high viscosities, for example a recently reported value of more than 2 Pa·s for the mixture of LCO and Ketjen additive, and thus high pumping energy demands are necessary to flow such a slurry [34]. From a performance perspective, the rheological properties of the suspension will impact the distribution of particles in the suspension, the access of material to the current collector, and the collision frequency and residence time for the particles in contact with the current collector. Based on previous studies [60, 61],

various factors contribute to the rheological behavior, such as particle size and morphology, salt concentration, temperature and pressure, and particle loading. Thus, considering the critical influence of particle loading on both rheological properties and the energy density of the suspension, we measured the viscosity of our LTO particle suspensions as a function of applied shear at a variety of particle loadings.

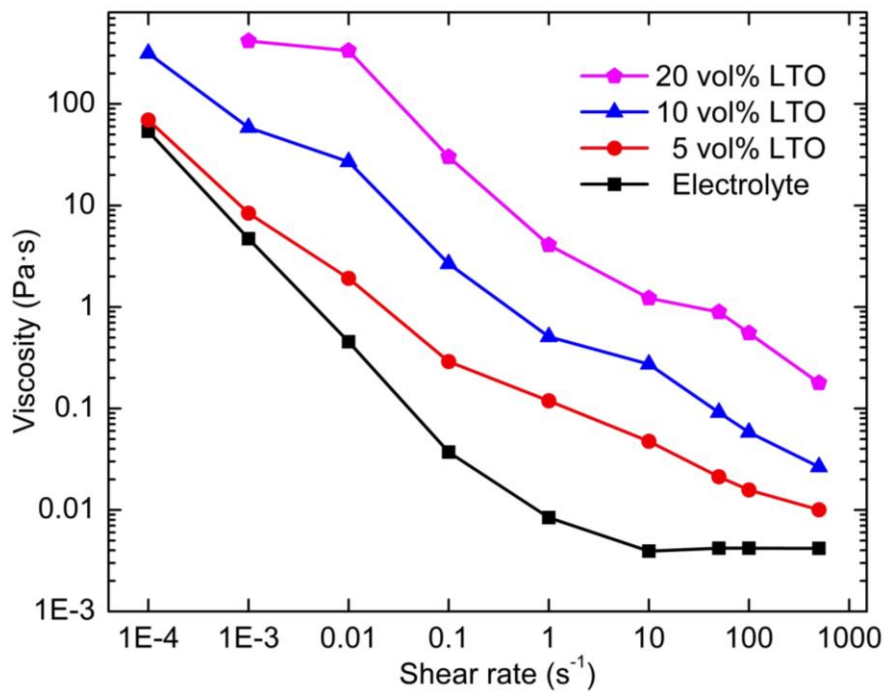


Figure 10. The viscosity as a function of shear rate for the particle-free electrolyte (1.2 M LiPF₆ in EC/EMC = 3:7 solvents, black squares) and the electrolyte laden with 5 (red circles), 10 (blue triangles), and 20 (purple pentagons) vol% LTO.

Figure 10 displays the viscosity as a function of shear rate for the particle-free electrolyte (1.2 M LiPF₆ in EC/EMC = 3:7 solvents as described in the Experimental section) and the electrolyte laden with 5, 10, and 20 vol% LTO. The electrolyte both with and without particles displayed shear-thinning behavior, with

the viscosity decreasing with increasing shear rate [60]. The particle-free electrolyte showed a Newtonian behavior with a flat plateau at shear rates higher than 10 s^{-1} [60]. The viscosity for all samples changed multiple orders of magnitude over the shear range investigated. We also noted that the viscosity increased with a higher LTO loading. For the lowest particle concentration of 5 vol%, the measured viscosity was close to that of the particle-free electrolyte at low shear rates. The drag force provided by the LTO particles in the electrolyte became more pronounced at higher shear rates. This behavior indicates that at the lowest concentration (5 vol%), the LTO particles had only a minor influence on the viscosity of the fluid dispersion. However, at 10 and 20 vol% LTO concentration, the viscosities were significantly higher than particle-free electrolyte and 5 vol% LTO within the whole range of applied shear. Also, the Newtonian plateau at higher shear rate disappeared, and instead an extended shear-thinning behavior was observed when LTO was dispersed at the two higher concentrations. This behavior is consistent with the extreme shear-thinning behavior of flocculated metal oxide suspensions [62, 63] and previous research on LTO suspensions, which have reported that the flocculated network breaks up into smaller flocculates after sufficient shear, resulting in the steep decrease in viscosity [61].

The relation between the viscosity and shear rate in the shear thinning region can be described by a power law or Ostwald–de Waele relationship [64], taking the form of Equation 5, where η is the viscosity, $\dot{\gamma}$ is the shear rate, and K and n

are fitting parameters. K is known as the flow consistency index, giving the viscosity at a shear rate of 1 s^{-1} . The dimensionless power law index describes the behavior compared with a Newtonian fluid. For a Newtonian fluid, $n = 1$; for a shear-thinning fluid, $n < 1$ and for a shear-thickening fluid n is greater than 1.

$$\eta = K\dot{\gamma}^{n-1} \quad (5)$$

Experimental data from the LTO suspensions in Figure 5 were used to obtain the fitting parameters K and n . The fits of the 5 vol% LTO suspension was $K = 0.18$ and $n = 0.44$ ($R^2 = 0.98$); the 10 vol% LTO suspension was $K = 0.96$ and $n = 0.39$ ($R^2 = 0.99$); and the 20 vol% LTO suspension was $K = 7.80$ and $n = 0.38$ ($R^2 = 0.97$). These results and the quality of the fitting parameters further confirmed the shear-thinning behavior of the LTO suspensions [60]. The increasing K values with increased particle loadings indicated that suspensions with higher loadings generally have greater viscosities as would be expected; however, the decreasing n values with increased particle loading indicated that suspensions with higher loadings have more extensive shear-thinning behavior. The greater shear thinning with increased particle loading is consistent with the higher loading being more flocculated, with the flocs becoming less stable and breaking up with sufficient applied shear. We also note that the n values are very close for 10 vol% and 20 vol% LTO, indicating that the transition to a more flocculated suspension occurs between 5 vol% and 10 vol% LTO. The observed shear-thinning is important to the operation of a solid dispersion flow battery, because the rheological data indicate that there will be advantages from a perspective of reducing the suspension viscosity to operating at higher shear

rates. A higher shear rate of the suspension means a higher flow rate in the tubing and the electrochemical channels of a flow cell. While the flow battery cannot be operated at an arbitrarily high flow rate, operation beyond the limit where flocs break up would be desirable from the standpoint of reducing suspension viscosity. Also, the increases in viscosity for higher LTO concentration means that there is a trade off in the flow cell between energy density and energy efficiency. Future studies will be conducted to understand the structure of the particle aggregates and the conditions that control the onset of the flocculation.

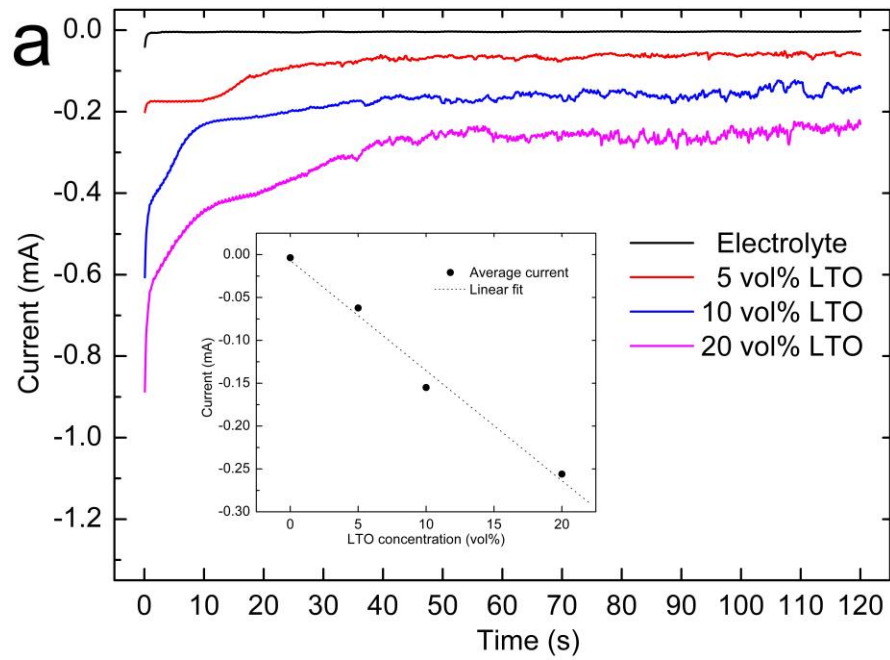
3.5. Vial Cell Electrochemical Characterization

In advance of constructing a full flow cell to characterize the dispersed particle electrolyte suspensions, a “vial cell” as described in the Experimental section was used to characterize our particle suspensions electrochemically. The advantages of the vial cell are that it is relatively less time consuming to construct than a flow cell and it is not susceptible to clogging of pumping elements because all of the particle contact with the current collector was implemented via stirring. As described previously, the particles were kept dispersed in the electrolyte in the vial cell via a rotating stir bar and electrochemical reactions occurred at the surface of an aluminum wire current collector. A piece of lithium foil, separated from the suspension by being wrapped in separator material, was used as the counter and reference electrode. To characterize the discharge of the LTO suspension, Chronoamperometry (CA) was performed for LTO

suspensions of different loadings. The primary objective of the vial cell experiments was to investigate the relationship between particle loading in the electrolyte and electrochemical activity.

For the vial cell CA experiments, a fixed discharge potential of 1.2 V was used and the current was measured for 120 seconds. This voltage was chosen because it was below the 1.55 V typical discharge plateau of LTO, but above the potential where electrolyte decomposition and lithium aluminum alloy formation would be expected to compete with lithium intercalation for the currents measured [65-67]. The short measuring time of 120 s was chosen because it was enough to observe a stable current output and time-efficient to perform the tests. The results of CA using the vial cell for increasing particle loadings in the electrolyte dispersions can be found in Figure 11a. The electrolyte without particles dispersed was used as a control, and as expected the measured current was very low, with the steady-state value approaching 0 mA. Compared with the electrolyte, all the other samples achieved a measureable current output (the currents were negative because the cell was discharging). Therefore, the LTO particles in the suspension were the source of the observed electrochemical activity. To further understand if the reactions were caused by lithium insertion into the LTO particles, cyclic voltammetry (CV) testing was performed for these suspensions in the vial cell at 5 mV s^{-1} and the results are shown in Figure 11b. The reduction and oxidation peaks were around 1.55 V. No other peaks were observed, indicating no other major redox reactions were occurring in the vial cell

system except for the desired oxidation/reduction of LTO. The electrochemical responses that were observed could have been caused either by LTO particles attached on the aluminum wire or by the particles in the suspension colliding with the aluminum wire.



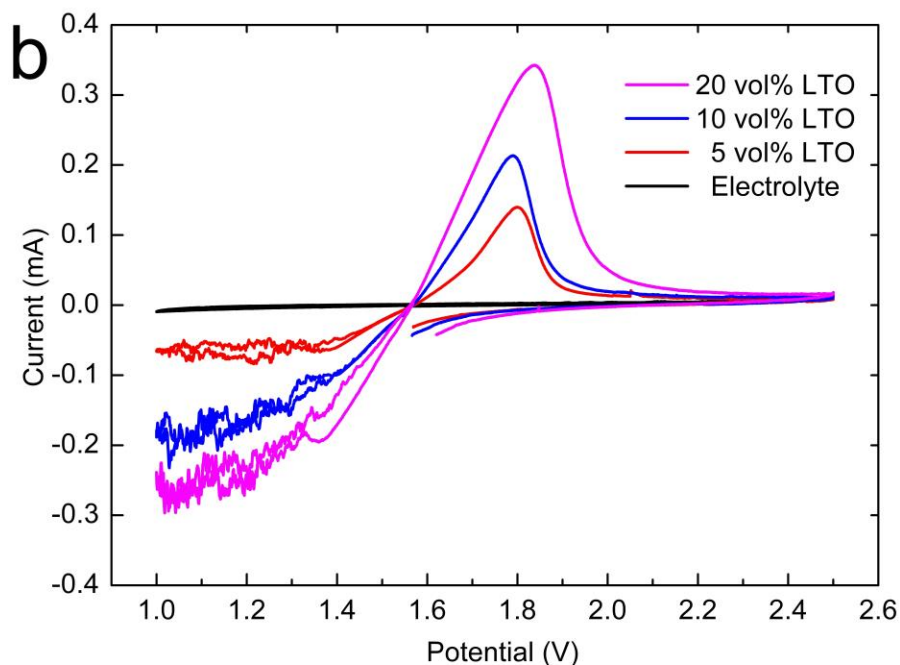
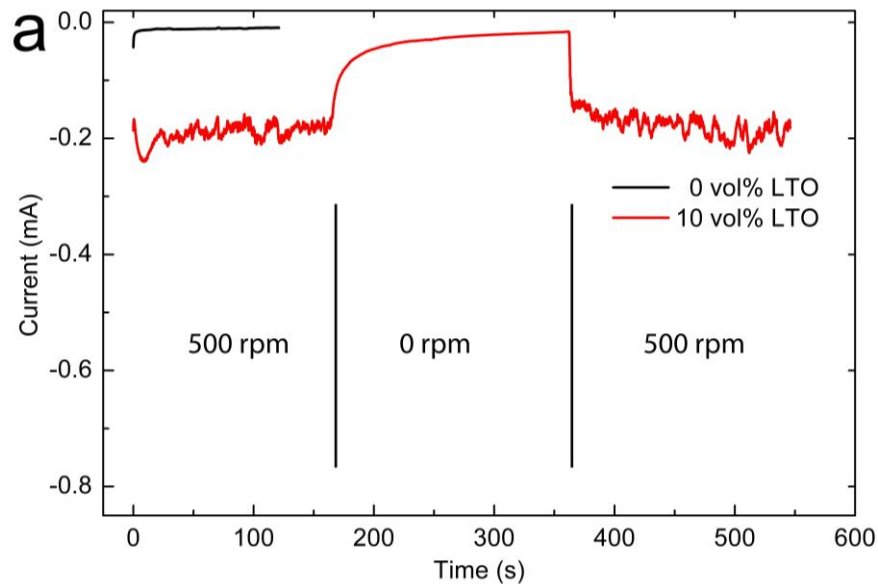


Figure 11. (a) Chronoamperometry (CA) profiles at 1.2 V and (b) cyclic voltammetry (CV) scans at the rate of 5 mV s^{-1} for the particle-free electrolyte and the electrolyte laden with 5 (red), 10 (blue), and 20 (purple) vol% LTO as measured in the vial cell. Inset in (a) is the steady state current as a function of the LTO concentration in the suspension.

To provide insights into whether electrochemical activity originated from attached or colliding LTO particles, a CA test was performed in the vial cell where the suspension stirring was halted during the test. If the electrochemical activity was from adsorbed particles, the current signal would be expected to remain approximately constant, while if the current was due to colliding particles we expected the measured current to drop to approximately zero due to the absence of stirring initiating particle collisions with the current collector. This CA experiments was conducted at 1.2 V with the 10 vol% LTO suspension. As

shown in Figure 12a, when the stirring was stopped at ~ 160 s, the current response quickly dropped to the background level. The measured current increased back to ~ 0.2 A as the stirring was resumed at ~ 360 s. The results in Figure 12a demonstrate that the discharge current from the LTO suspension is dependent on the agitation of the solution provided by stirring. The results above lead us to conclude that the electrochemical reactions observed were due to lithium insertion and extraction into/out of LTO particles as they collided with the aluminum wire current collector and that statically adsorbed LTO particles on the current collector provided a negligible contribution to the observed electrochemical reactions, at least after sufficient timescales to discharge the adsorbed particles.



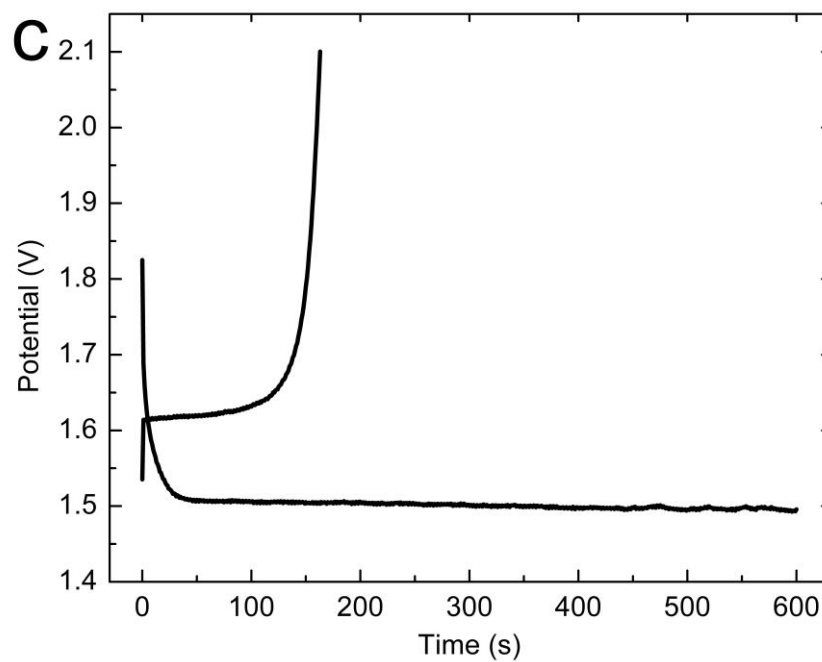
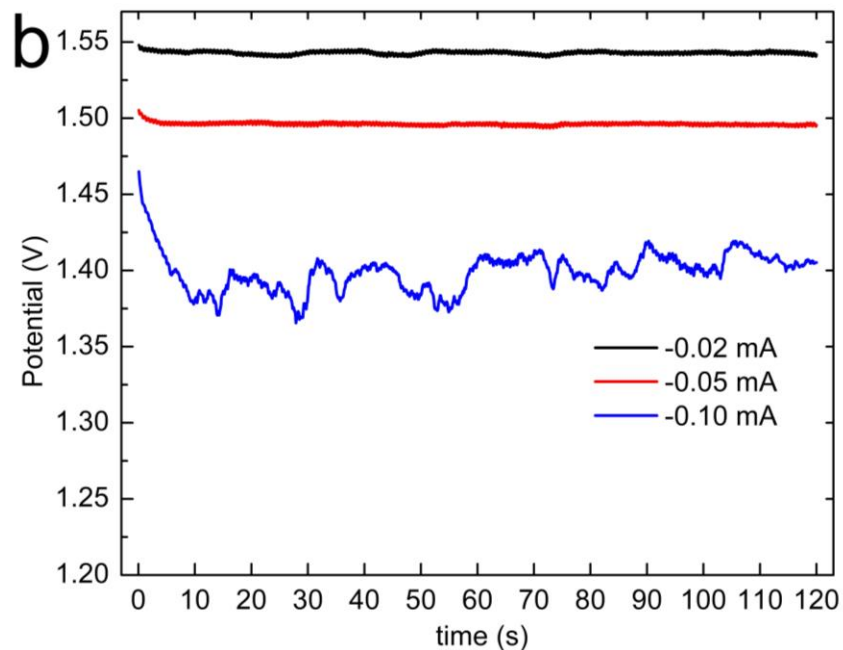


Figure 12. (a) Chronoamperometry (CA) profiles at 1.2 V with the stirring halted during the test, (b) Chronopotentiometry (CP) profiles with applied discharge currents 0.02, 0.05, 0.10 mA, and (c) discharge and charge curves for the vial cell with an LTO concentration of 10 vol%.

As shown in the insert of Figure 11a, the discharge current linearly increased with the LTO concentration. This dependence of the measured CA current on LTO loading could be caused by the change in the collision frequencies of LTO particles on the aluminum wire for increased LTO loading. In the simplest case where the LTO particles were discrete units, a higher LTO concentration would provide more LTO particles within the range of the electron transfer distance from the aluminum wire, and hence more LTO particles would be able to collide on the aluminum wire and subsequently were discharged, resulting in the increased observed output currents. In addition, as discussed previously, rheological data suggested a more flocculated particle structure formed as the suspended particle concentration was increased. The flocculated aggregates would promote inter-particle charge transfer, further increasing the discharge current. The idea of inter-particle charge transfer providing electrochemical capacity from particles not in direct contact with the current collector is further supported by the results from our particle coin cells, which indicated LTO particles far from the current collector contributed to the electrochemical capacity of the cell. The electrochemical plateaus had surprisingly little noise in the measured current for the first ~ 20 s of each CA curve, especially when compared to the steady-state current. This behavior was attributed to the electrochemical activity of a small amount of LTO powder attached on the aluminum wire. These attached particles were discharged as soon as the test started and were fully discharged quickly due to their small total capacity in the system. The steady-state current plateau; however, was attributed to the electrochemical discharge of LTO particles from

the suspension colliding with the aluminum surface. We note that the CA curves were not flat but had fluctuations in the measured current. We attribute the fluctuations of the CA curves to the LTO particles not being perfectly homogeneously dispersed within the electrolyte. Thus, the concentration of LTO particles near the current collector, as well as number of particles/aggregates in direct contact, varies at any given instant. This local inhomogeneity in the dispersion results in the fluctuation in the observed current because when more total particles/aggregates were in contact with the current collector, greater electrochemical current was produced.

The CV curves in Figure 11b also were influenced by the LTO concentration in the suspension. The CV results were consistent with the CA measurements from the perspective that there was an increase in the measured current as the LTO loading was increased. During electrochemical reduction of the LTO in the CV scan, a typical CV peak is not observed. These CV scans were not taken in quiescent solution, but instead were in a highly turbid constantly stirred suspension. We attribute the lack of a reduction peak and the increased noise in the measured current at lower voltages on reduction to the electrochemical reactions in this regime being limited by the collision rate of particles in the suspension with the current collector wire. An interesting phenomenon observed in the CV curves was that there were significant oxidation peaks, even though only a very small fraction of the LTO particles (which initially should all be in the oxidized state) have been reduced. We estimate the fraction of the LTO material

in the suspension that has been reduced before the oxidation half cycle to be only $< 0.01\%$ of the total electrochemical capacity within the dispersion. Thus, the significant LTO oxidation peaks in the CV scans indicate that some of the same LTO particles that participated in electrochemical reduction were still available to collide with the aluminum current collector and participate in electrochemical oxidation reactions on the aluminum wire current collector. This may be because the LTO particles were first discharged on the surface layer and refreshed before being expelled to inner layers [68], thus the number of particles that were discharged on the surface was much more than 0.01% of the total number of particles, even though the mass of total material that was discharged was less than 0.01% of the total capacity based on the LTO mass available. In addition, the discharged/lithiated LTO particles had a much higher conductivity than fully charged particles, thus the partially discharged LTO will have a relatively low resistance to electron transfer, in particular relative to the fully charged LTO [68-70]. Thus, even though only a small mass proportion of LTO was discharged, the observed oxidation peak was still significant. The inter-particle charge transfer, as discussed previously, may also contribute to the observed LTO oxidation. The polarization of the CV curves was observed to be independent of loading of LTO particles. Great care was taken to use the same aluminum wire, lithium foil, and the wire-foil separation for all measurements at the different loadings and hence the IR drop associated with these components would be expected to be equivalent for all the measurements [71].

To further characterize the discharging behavior of the vial cell system, chronopotentiometry (CP) testing was performed for the 10 vol% sample with aluminum wire as the working electrode and lithium foil as the counter and reference electrode. For currents of -0.02, -0.05, and -0.10 mA, the potentials measured for the vial cell are shown in Figure 12b. Decreasing steady-state potentials were observed as the current was increased, consistent with previous reports [41, 53, 72-74]. The observed behavior was attributed to the increased IR drop in the vial cell with increasing current. The open cell voltage (OCV) was measured to be 1.57 V, and the steady-state potentials for 0.02, 0.05 and 0.10 mA discharge currents acquire were 1.54, 1.49 and 1.40 V, respectively. These results were consistent with an almost linear decreasing relationship of the IR drop with increasing current. We note that the CP curve for the 0.10 mA test was relatively unstable compared to the 0.02 mA and 0.05 mA currents. We speculate that at 0.10 mA we are starting to reach the limits of the stable current that we can draw for the stochastic particle collision process, at least for the level of agitation and amount of exposed surface area on the current collector in the vial cell as was constructed for the measurement.

Constant current discharging and charging was performed with the vial cell to demonstrate the viability of charging and discharging the vial cell as a battery. The constant current charge/discharge tests were performed using the 10 vol% dispersion. As shown in Figure 12c, the cell was first discharged at 0.05 mA for 10 minutes and was then switched over to charge at 0.05 mA, with the cell being

successfully charged for 3 minutes before hitting the upper voltage cut-off of 2.1 V. The charge and discharge plateaus were both at ~ 1.55 V, consistent with lithium insertion and extraction into/out of LTO particles with low polarization [40, 41, 51-53]. While the total capacities charged/discharged were relatively low (the total discharge capacity was 8.33×10^{-3} mAh and the total charge capacity was 3.18×10^{-3} mAh, corresponding to $< 0.01\%$ of the capacity of the LTO particles in the suspension), full discharge and charge of the cell would have been impractical because of the relatively low current densities in the vial cell. The coulombic efficiency also appears artificially low because most of the discharged material was exchanged into the solution laden with LTO particles in the oxidized state, limiting the total capacity available. The primary purpose of the test was to demonstrate 1) that the vial cell was capable of charge and discharge with colliding LTO particles, and 2) that the polarization during charge and discharge was low. Both of these principles were demonstrated in the vial cell, and thus we moved to finally demonstrating electrochemical capacity of the LTO suspension within a custom flow cell geometry.

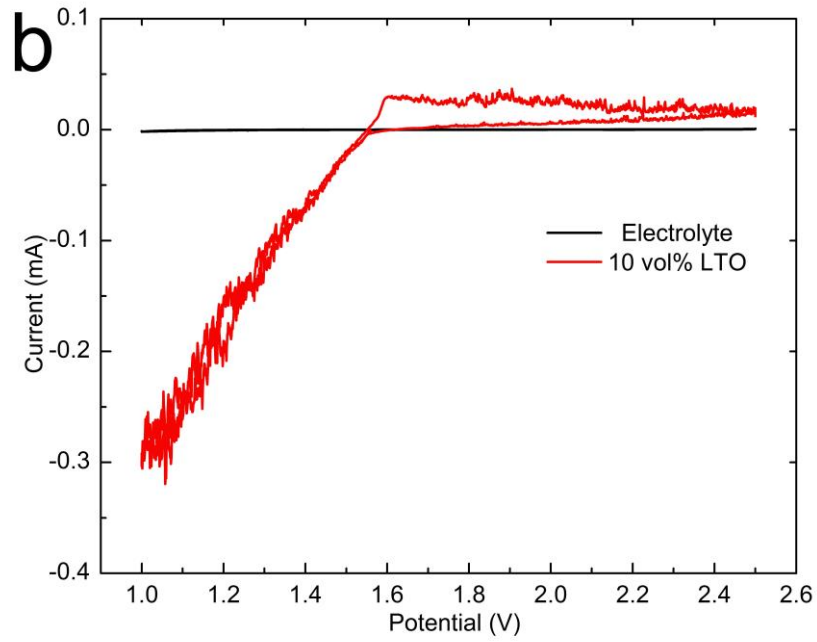
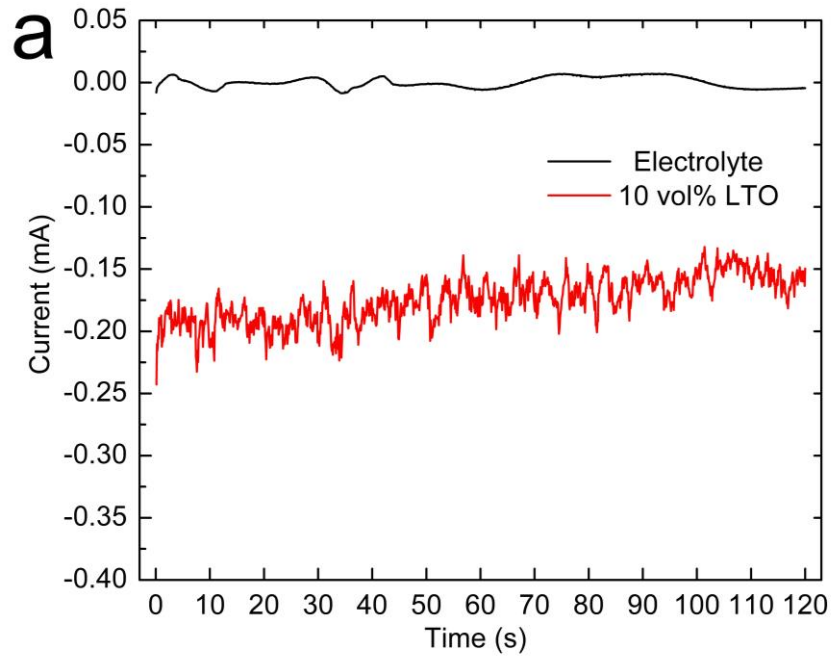
3.6. Flow Cell Electrochemical Characterization

Although the vial cell system provided insights into the electrochemical properties of LTO suspensions, a flow cell was constructed to demonstrate electrochemical capacity for the LTO suspensions in a flow battery system. We assembled a custom flow cell (Figure 5b) using the 10 vol% LTO suspension. The 10 vol% LTO suspension was chosen to minimize clogging the tubes that carried the

electrolyte while still providing adequate electrochemical capacity. The flow rate used for the LTO suspension through the flow channel and tubing was 120 mL min⁻¹.

A CA test was performed for the flow cell at a fixed potential of 1.2 V, the same potential used with the vial cells, and the results are shown in Figure 13a. The CA curve displayed similar behavior to that observed for the vial cell. The significant current measured in excess of the baseline confirmed that the LTO particles were discharged in the flow cell. CV was used to further confirm that there was electrochemical capacity from the LTO within the flow cell (Figure 8b). The redox peaks at ~ 1.55 V were consistent with the lithiation and delithiation of LTO particles [40, 41, 51-53]. Similar to the vial cell, the current output fluctuated due to the local inhomogeneity of the LTO suspension. The CV profile in the flow cell was similar to the vial cell, although the oxidation peak was much smaller. This was because the amount of LTO material in the flow cell experiment was larger than the amount used in the vial cell, while the surface area available from the current collector was less, resulting in a decrease in the relative amount of LTO particles discharged. This difference in cell geometry resulted in the absence of an LTO oxidation peak because of the limited amount of discharged LTO particles in the flow channel. In the flow cell, the oxidation current was smaller relative to the vial cell because a much smaller portion of LTO particles were discharged; and the “peak” was broadened because the residence time

was short and the reaction was not limited by lithium-ion diffusion but rather by the available discharged LTO particle concentration.



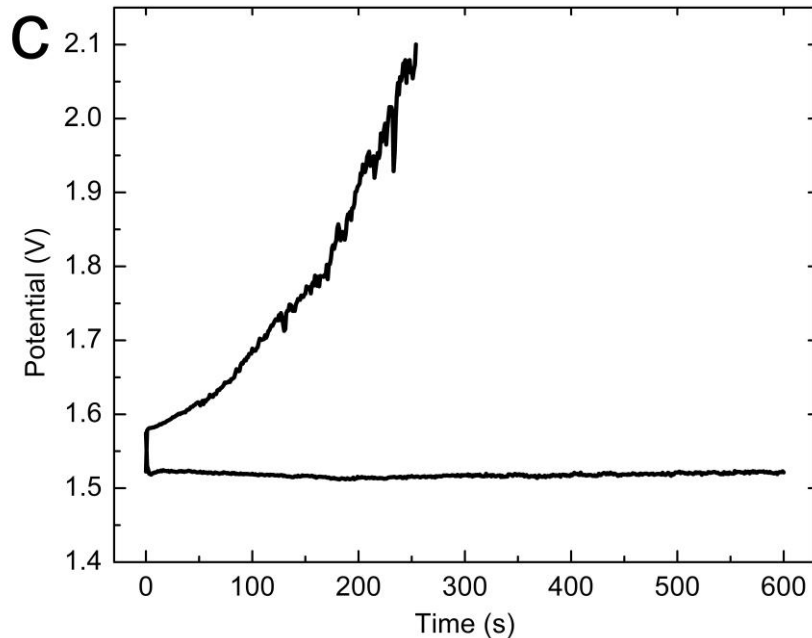


Figure 13. (a) Chronoamperometry (CA) profile at 1.2 V, (b) cyclic voltammetry (CV) scan at the rate of 5 mV s^{-1} , and (c) discharge and charge curve for the flow cell with an LTO concentration in the electrolyte of 10 vol%.

A constant current discharge and charge was also performed for the same 10 vol% sample (Figure 13c). The profile used was similar to the vial cell described previously. A constant current discharge was performed at 0.02 mA for 10 minutes, followed by a constant current charge at 0.02 mA that reached the upper voltage cut-off after ~ 4 minutes. The discharge plateau was at $\sim 1.55 \text{ V}$, and the charge cycle starts at a plateau at $\sim 1.55 \text{ V}$ before quickly increasing in potential. The capacities were of $3.33 \times 10^{-3} \text{ mAh}$ for discharge and $1.49 \times 10^{-3} \text{ mAh}$ on charge. It is not surprising that only a fraction of the discharge capacity is recovered on charge, as a very small portion of LTO particles were discharged. Interestingly, the columbic efficiency of the flow cell was higher than what was observed for the vial cell. This may have been due to the lower current used with

the flow cell test (0.02 mA) compared to the vial cell test (0.05 mA). Also, we note that the charging curve has more noticeable fluctuations and a greater polarization relative to the vial cell. This is because the vial cell had constant access to the discharged particles during testing while the flow cell was only able to charge the small portion of the discharged particles that was in the flow chamber at any given time. While the capacities obtained in this cell are relatively modest, they successfully demonstrate the galvanic cycling of a solid dispersion LTO flow battery that relies on collision of LTO particles with the current collector to store and deliver electrochemical energy. Future efforts will be taken to increase the power of the cell to achieve full discharge and charge cycles within practical time limits.

It is instructive to discuss the solid dispersion flow system relative to existing flow battery systems. Assuming that we can achieve capacities for the LTO in our LTO dispersions comparable what was reversibly measured for our LTO particle coin cells, the anolyte within our flow cell setup would be able to achieve a capacity of 55.6 mAh g⁻¹ (total anolyte mass basis) with a viscosity of ~ 0.17 Pa·s at 20 vol% LTO loading. Some of the highest reported vanadium anolyte concentrations for vanadium redox flow batteries have theoretical capacities and viscosities within a similar range [75], however, the dispersion flow battery has the advantages of the ability to pair our anolyte with higher voltage lithium-ion catholyte materials and we are exploring the possibility of increasing LTO particle loading which would result in an even higher capacity dispersion. Also, relative to

the semi-solid flow battery systems reported in the literature [34], for similar particle volume loadings of particles the solid dispersion flow battery system reported here operates without carbon additives and has a much lower viscosity. The energy density for the solid dispersion flow battery is only dependent on the energy density of the solid active material itself and the volume fraction of the active material that can be stably dispersed and efficiently pumped.

4. Conclusions and Recommendations

A Solid Dispersion Flow Battery consisting of an organic lithium-ion electrolyte laden with $\text{Li}_4\text{Ti}_5\text{O}_{12}$ (LTO) was demonstrated and characterized electrochemically with a unique and systematic approach. It was found that LTO-to-LTO particle contacts provide sufficient electronic conductivity to allow particles multiple LTO particle distances from the current collector to contribute to battery capacity. The LTO suspension has a shear-thinning behavior and the current output of the LTO suspensions was linearly dependent on the LTO concentration. Electrochemical characterization of LTO dispersions in custom flow geometries indicates electrochemical capacity is provided by collision of LTO particles with the current collector, and that design of a flow cell relying on collision from a particle dispersion can be successfully reversibly electrochemically oxidized and reduced. The characterization methods described in this work provide a systematic step-by-step method to study flow batteries.

A Solid Dispersion Flow Battery system inherits the advantages of conventional redox flow batteries to decouple the power and the energy in the system, providing the flexibility to independently adjust and design the power and energy requirements for an application. This system also has the potential to provide a much higher energy density with a lower viscosity comparing with vanadium flow battery and semi-solid flow battery, provided that the anolyte described in this study can be paired with a suitable catholyte. To further develop the technology, the catholyte will follow the same design of the LTO anolyte. The cathode

material particles will be dispersed in the same electrolyte to serve as the counter electrode. To cycle the full cell, both the catholyte and the anolyte will be pumped through the electrochemical cell with aluminum current collectors on each side and a separator in between, similar as a redox flow battery. Future research efforts will also need to be done to improve the power output of the solid dispersion flow battery. Because even though this work demonstrated this type of flow battery, the power output is relatively low.

5. References

- [1] Z. Yang, J. Zhang, M.C. Kintner-Meyer, X. Lu, D. Choi, J.P. Lemmon, J. Liu, *Chem Rev*, 111 (2011) 3577-3613.
- [2] C.o.A.s.E. Future, N.A.o. Sciences, N.A.o. Engineering, N.R. Council, *America's Energy Future: Technology and Transformation: Summary Edition*, The National Academies Press, Washington, DC, 2009.
- [3] A.Z. Weber, M.M. Mench, J.P. Meyers, P.N. Ross, J.T. Gostick, Q. Liu, *Journal of Applied Electrochemistry*, 41 (2011) 1137-1164.
- [4] C.J. Yang, R.B. Jackson, *Renew Sust Energ Rev*, 15 (2011) 839-844.
- [5] B. Dunn, H. Kamath, J.M. Tarascon, *Science*, 334 (2011) 928-935.
- [6] L. Lu, X. Han, J. Li, J. Hua, M. Ouyang, *J Power Sources*, 226 (2013) 272-288.
- [7] H. Kim, D.A. Boysen, J.M. Newhouse, B.L. Spatocco, B. Chung, P.J. Burke, D.J. Bradwell, K. Jiang, A.A. Tomaszowska, K. Wang, W. Wei, L.A. Ortiz, S.A. Barriga, S.M. Poizeau, D.R. Sadoway, *Chem Rev*, 113 (2013) 2075-2099.
- [8] M.A. Rahman, X. Wang, C. Wen, *Journal of Applied Electrochemistry*, 44 (2013) 5-22.
- [9] S. Xin, Y.X. Yin, Y.G. Guo, L.J. Wan, *Advanced materials*, 26 (2014) 1261-1265.
- [10] B.C. Duan, W.K. Wang, A.B. Wang, Z.B. Yu, H.L. Zhao, Y.S. Yang, *J Mater Chem A*, 2 (2014) 308-314.
- [11] A. Manthiram, K. Chemelewski, E.-S. Lee, *Energ Environ Sci*, 7 (2014) 1339.
- [12] M. Armand, J.M. Tarascon, *Nature*, 451 (2008) 652-657.
- [13] M.S. Whittingham, *Chemical reviews*, 104 (2004) 4271-4301.
- [14] J.W. Fergus, *Journal of Power Sources*, 195 (2010) 939-954.
- [15] D. Ensling, G. Cherkashinin, S. Schmid, S. Bhuvaneswari, A. Thissen, W. Jaegermann, *Chemistry of Materials*, 26 (2014) 3948-3956.
- [16] G.J. Suppes, B.D. Sawyer, M.J. Gordon, *Aiche J.*, 57 (2011) 1961-1967.
- [17] S.F. Schuster, M.J. Brand, P. Berg, M. Gleissenberger, A. Jossen, *J Power Sources*, 297 (2015) 242-251.
- [18] R. Mahamud, C. Park, *J Power Sources*, 196 (2011) 5685-5696.
- [19] S.M. Rezvanizani, Z. Liu, Y. Chen, J. Lee, *J Power Sources*, 256 (2014) 110-124.
- [20] W. Waag, C. Fleischer, D.U. Sauer, *J Power Sources*, 258 (2014) 321-339.
- [21] C.P. de Leon, A. Frias-Ferrer, J. Gonzalez-Garcia, D.A. Szanto, F.C. Walsh, *J Power Sources*, 160 (2006) 716-732.
- [22] A. Parasuraman, T.M. Lim, C. Menictas, M. Skyllas-Kazacos, *Electrochimica Acta*, 101 (2013) 27-40.
- [23] M.H. Chakrabarti, N.P. Brandon, S.A. Hajimolana, F. Tariq, V. Yufit, M.A. Hashim, M.A. Hussain, C.T.J. Low, P.V. Aravind, *J Power Sources*, 253 (2014) 150-166.
- [24] X. Ke, J.I.D. Alexander, J.M. Prah, R.F. Savinell, *J Power Sources*, 270 (2014) 646-657.
- [25] L. Yue, W.S. Li, F.Q. Sun, L.Z. Zhao, L.D. Xing, *Carbon*, 48 (2010) 3079-3090.
- [26] M.S. Park, N.J. Lee, S.W. Lee, K.J. Kim, D.J. Oh, Y.J. Kim, *ACS applied materials & interfaces*, 6 (2014) 10729-10735.

- [27] X.J. Wu, S.Q. Liu, N.F. Wang, S. Peng, Z.X. He, *Electrochimica Acta*, 78 (2012) 475-482.
- [28] C.X. Sun, J. Chen, H.M. Zhang, X. Han, Q.T. Luo, *J Power Sources*, 195 (2010) 890-897.
- [29] D. Pletcher, R. Wills, *Phys Chem Chem Phys*, 6 (2004) 1779-1785.
- [30] Y.F. Zhao, S.H. Si, L. Wang, P. Tang, H.J. Cao, *Journal of the Electrochemical Society*, 161 (2014) A330-A335.
- [31] M. Gordon, G. Suppes, *Aiche J.*, 59 (2013) 2833-2842.
- [32] M. Gordon, G. Suppes, *Aiche J.*, 59 (2013) 1774-1779.
- [33] Y. Ding, Y. Zhao, G. Yu, *Nano letters*, (2015).
- [34] M. Duduta, B. Ho, V.C. Wood, P. Limthongkul, V.E. Brunini, W.C. Carter, Y.M. Chiang, *Adv. Energy Mater.*, 1 (2011) 511-516.
- [35] Z. Li, K.C. Smith, Y.J. Dong, N. Baram, F.Y. Fan, J. Xie, P. Limthongkul, W.C. Carter, Y.M. Chiang, *Phys Chem Chem Phys*, 15 (2013) 15833-15839.
- [36] S. Hamelet, T. Tzedakis, J.B. Leriche, S. Sailler, D. Larcher, P.L. Taberna, P. Simon, J.M. Tarascon, *Journal of the Electrochemical Society*, 159 (2012) A1360-A1367.
- [37] L. Madec, M. Youssry, M. Cerbelaud, P. Soudan, D. Guyomard, B. Lestriez, *Chempluschem*, 80 (2015) 396-401.
- [38] V.E. Brunini, Y.-M. Chiang, W.C. Carter, *Electrochimica Acta*, 69 (2012) 301-307.
- [39] V. Viswanathan, A. Crawford, D. Stephenson, S. Kim, W. Wang, B. Li, G. Coffey, E. Thomsen, G. Graff, P. Balducci, M. Kintner-Meyer, V. Sprenkle, *J Power Sources*, 247 (2014) 1040-1051.
- [40] S. Deng, J. Li, S. Sun, H. Wang, J. Liu, H. Yan, *Electrochimica Acta*, 146 (2014) 37-43.
- [41] N.D. He, B.S. Wang, J.J. Huang, *J Solid State Electr*, 14 (2010) 1241-1246.
- [42] Z. Yang, D. Choi, S. Kerisit, K.M. Rosso, D. Wang, J. Zhang, G. Graff, J. Liu, *J Power Sources*, 192 (2009) 588-598.
- [43] T. Ohzuku, A. Ueda, N. Yamamoto, *J. Electrochem. Soc*, 142 (1995).
- [44] T. Ohzuku, A. Ueda, *Solid State Ionics*, 69 (1994).
- [45] I. Belharouak, G.M. Koenig, K. Amine, *J Power Sources*, 196 (2011) 10344-10350.
- [46] D. Tsubone, T. Hashimoto, K. Igarashi, T. Shimizu, *J. Ceram. Soc. Jpn. Inter. Ed.*, 102 (1994).
- [47] J. Hanawalt, et al., *Anal. Chem.*, 10 (1938).
- [48] T. Yuan, R. Cai, R. Ran, Y. Zhou, Z. Shao, *J Alloy Compd*, 505 (2010) 367-373.
- [49] Y. Shen, M. Søndergaard, M. Christensen, S. Birgisson, B.B. Iversen, *Chemistry of Materials*, 26 (2014) 3679-3686.
- [50] S.K. Martha, O. Haik, V. Borgel, E. Zinigrad, I. Exnar, T. Drezen, J.H. Miners, D. Aurbach, *Journal of the Electrochemical Society*, 158 (2011) A790-A797.
- [51] Z. He, Z. Wang, F. Wu, H. Guo, X. Li, X. Xiong, *J Alloy Compd*, 540 (2012) 39-45.
- [52] T.-F. Yi, S.-Y. Yang, M. Tao, Y. Xie, Y.-R. Zhu, R.-S. Zhu, *Electrochimica Acta*, 134 (2014) 377-383.
- [53] C.F. Lin, X.Y. Fan, Y.L. Xin, F.Q. Cheng, M.O. Lai, H.H. Zhou, L. Lu, *Nanoscale*, 6 (2014) 6651-6660.
- [54] P. Kubiak, M. Pfanzelt, J. Geserick, U. Hörmann, N. Hüsing, U. Kaiser, M. Wohlfahrt-Mehrens, *J Power Sources*, 194 (2009) 1099-1104.

- [55] J.-W. Shin, C.-H. Hong, D.-H. Yoon, N. Dudney, *Journal of the American Ceramic Society*, 95 (2012) 1894-1900.
- [56] M.S. Song, A. Benayad, Y.M. Choi, K.S. Park, *Chem Commun*, 48 (2012) 516-518.
- [57] C. Kim, N.S. Norberg, C.T. Alexander, R. KostECKI, J. Cabana, *Advanced Functional Materials*, 23 (2013) 1214-1222.
- [58] D. Young, A. Ransil, R. Amin, Z. Li, Y.M. Chiang, *Adv. Energy Mater.*, 3 (2013) 1125-1129.
- [59] M. Park, X. Zhang, M. Chung, G.B. Less, A.M. Sastry, *J Power Sources*, 195 (2010) 7904-7929.
- [60] J. Mewis, N.J. Wagner, *Colloidal suspension rheology*, Cambridge University Press, Cambridge, UK New York, 2012.
- [61] M. Youssry, L. Madec, P. Soudan, M. Cerbelaud, D. Guyomard, B. Lestriez, *J Power Sources*, 274 (2015) 424-431.
- [62] T.L. Smith, C.A. Bruce, *Journal of Colloid and Interface Science*, 72 (1979).
- [63] Z. Zhou, P.J. Scales, D.V. Boger, (2000).
- [64] W. Ostwald, *Kolloid-Zeitschrift*, 47 (1929) 176 - 187.
- [65] X. Zhang, T.M. Devine, *Journal of The Electrochemical Society*, 153 (2006) B344.
- [66] S.-T. Myung, H. Yashiro, *J Power Sources*, 271 (2014) 167-173.
- [67] M. Morita, T. Shibata, N. Yoshimoto, M. Ishikawa, *Electrochimica Acta*, 47 (2002).
- [68] N. Takami, H. Inagaki, T. Kishi, Y. Harada, Y. Fujita, K. Hoshina, *Journal of The Electrochemical Society*, 156 (2009) A128.
- [69] W. Schmidt, P. Bottke, M. Sternad, P. Gollob, V. Hennige, M. Wilkening, *Chemistry of Materials*, 27 (2015) 1740-1750.
- [70] N. Takami, K. Hoshina, H. Inagaki, *Journal of the Electrochemical Society*, 158 (2011) A725-A730.
- [71] C.H. Hamann, A. Hamnett, W. Vielstich, *Electrochemistry*, 2 ed., Wiley-VCH, 2007.
- [72] L. Madec, M. Youssry, M. Cerbelaud, P. Soudan, D. Guyomard, B. Lestriez, *Journal of the Electrochemical Society*, 161 (2014) A693-A699.
- [73] X. Bai, T. Li, C. Wei, Y.-K. Sun, Y.-X. Qi, H.-L. Zhu, N. Lun, Y.-J. Bai, *Electrochimica Acta*, 155 (2015) 132-139.
- [74] J. Liu, K. Song, P.A. van Aken, J. Maier, Y. Yu, *Nano letters*, 14 (2014) 2597-2603.
- [75] F. Rahman, M. Skyllas-Kazacos, *J Power Sources*, 189 (2009) 1212-1219.